Earthquakes and Structures, *Vol. 19, No. 1 (2020) 1-16*
DOI: https://doi.org/10.12989/eas.2020.19.1.1

Dynamic interaction effects of buried structures on seismic response of surface structures

Rafet Sisman* and Yusuf Ayvaz

Department of Civil Engineering, Yildiz Technical University, Davutpasa Campus, Esenler, Istanbul, Turkey

(Received March 25, 2020, Revised May 20, 2020, Accepted June, 10, 2020)

Abstract. This study presents an investigation of the dynamic interactions between a surface structure lying on two different soil deposits and a square-shaped buried structure embedded in the soil. To this end, a large number of numerical models are generated by using a well-known Finite Element Method software, i.e., OpenSEES. The interaction phenomenon is assumed to be affected by six different parameters. In the parametric study, these parameters are assumed to have various values in accordance with the engineering practices. A total of 1620 possible combinations of the parameter values are addressed in this study. 30 different numerical models are also generated as the 'free-field cases' to set a reference. The surface structure drift and acceleration amplifications are used as a measure to evaluate the dynamic interactions. The response (i.e., drifts and accelerations) amplifications are calculated as the ratio of the maximum surface structure response in any 'case' to the maximum surface structure response in corresponding free-field case. Variation of the response amplifications with any of the investigated parameters is addressed in this paper. The results obtained from the numerical analyses clearly reveal that the presence of a buried structure in the vicinity of a surface structure can cause both amplification and de-amplification of the surface structure responses, depending on the case parameters.

Keywords: soil structure interaction; soft soil site; buried structure; surface structure

1. Introduction

Cities are densely populated places and still growing in terms of population. Many infrastructure facilities are constructed to meet the demands of that population. Thus, urban life is highly dependent on these facilities. Tunnels, buried pipelines, metro stations, and underground reservoirs can be listed among these facilities. In earthquake-prone regions, particular precautions may be required during the design of this kind of engineering structures. Besides seismic waves, the dynamic effects caused by the surface structures can also be important in the design of this kind of engineering structures.

A number of studies (Jafarnia and Varzaghani 2016, Pitilakis *et al*. 2014, Tsinidis 2018, Wang *et al*. 2017) from the literature investigated the dynamic interactions between surface structures and buried structures by utilizing numerical models. Besides numerical models, the interaction effect is also studied by using experimental setups (Wang *et al*. 2018). In these studies, dynamic effects on the buried structure responses due to presence of surface structures are examined. The researchers are always interested in this field due to the variability of the soil properties, surface structure properties and geometrical configuration of the problem.

On the other hand, seismic waves travel through soil layers to reach ground surface during earthquakes. During this propagation process, amplitudes of the seismic waves can be amplified or de-amplified. Also, the frequency content of those waves can be altered, depending on the mechanical and geometrical properties of the subsurface soil layers. Therefore, propagation of seismic waves through the soil layers should be taken into account during the design process of surface structures. For this purpose, soil site response analyses can be performed for the site where the surface structure is planned to be constructed.

There are a number of software that calculate soil site response, i.e. amplification or de-amplification due to the subsurface soil layers. However, to the best of authors' knowledge, none of those software takes underground anomalies into account. Underground reservoirs, buried culverts, tunnels, buried pipelines, and metro stations can be listed among those anomalies. As the seismic waves excite and effect this kind of buried structures, the buried structures also alter the amplitude and frequency content of the seismic waves. This mutual effect is an example of soil-structure interaction (SSI).

Besides soil site response, the underground structures can also alter the response of surface structures. A large number of studies from the literature investigated the inverse problem in terms of the ground surface responses. Various numerical methods are utilized in these studies, i.e. Boundary Element Method (Alielahi *et al*. 2015, Alielahi *et al*. 2016, Alielahi and Adampira 2016a, 2016b, Liang 2012), Finite Element Method (Rostami *et al*. 2016, Sica *et al*. 2014), Finite Difference Method (Baziar *et al*. 2014, Besharat *et al*. 2012, Yiouta-Mitra *et al*. 2007). Also analytical approaches (Smerzini *et al*. 2008, 2009) and experimental setups (Abuhajar *et al*. 2002, 2015, Baziar *et*

*Corresponding author, Ph. D. Candidate
E-mail: rafet@yildiz.edu.tr

ISSN: 2092-7614 (Print), 2092-7622 (Online)

al. 2016, Sgarlato *et al*. 2011) have been used to investigate the inverse problem. However, in these studies surface structures are not modelled or constructed (for experimental studies) directly. Instead, the researchers focused on the ground surface motions which would be used as input motions to the surface structures.

The surface structure response can be affected by the dynamic interaction between the underlying soil medium and itself. Thus, surface structures should be directly modelled in numerical studies. The differences in the surface structure response, between including and excluding surface structures in Finite Element Method (FEM) models, are given by Sisman and Ayvaz (2019a). A comprehensive study, in which the surface structure is modelled directly, is presented by Wang *et al*. (2013) to investigate the dynamic interaction effects due to presence of a nearby underground structure on a piled surface structure. Beyond the dynamic interaction, tunneling induced settlements of the ground surface and its effects on the nearby surface structures are also investigated (Franza *et al*. 2017, Lee *et al*. 2016, Zidan and Ramadan 2018). The case dependent nature of the problem leads researchers to carry out further studies in this field.

In this paper, it is aimed to illustrate the effects on the surface structure response due to the dynamic interaction between a square-shaped buried structure and a surface structure. This study focuses on the interaction phenomenon in case of soft and moderate soil conditions. For this purpose, two different soil sites are considered, which are representing soft and moderate soil conditions. On contrary to the previous studies from the literature, structural drift and acceleration amplifications caused by the interaction are given. The drift responses can be considered as an overall seismic demand measure for the surface structure design. On the other hand, the acceleration responses can be thought of as a seismic demand measure for non-structural components of the surface structure. A total of 1650 numerical analyses are performed in this study, 1620 of which correspond to different cases including a buried structure and a surface structure. Another 30 of which corresponds to different cases including only a surface structure. Detailed information about the case properties are given in the next section.

2. Case definitions

In this study, a large number of dynamic time history analyses are performed by using numerical models comprising of a soil deposit, a buried structure, and a surface structure. The analyses results are utilized to examine the interaction effects between the surface structure and the buried structure, with regard to several parameters. There are a number of parameters which are likely to affect this interaction, but only six of them are investigated in this study. The investigated parameters and parameter ranges are given in Table 1.

The depth ratio (R_D) parameter corresponds to the ratio of burial depth of the buried structure to its height. The burial depth and buried structure dimensions are shown in Fig. 1. The shape of the buried structure is selected to be a square, thus its width and height is always equal. It is done with the aim of controlling the dimensions of the square-shaped structure with only one parameter. The aspect ratio of the buried structure (i.e., the ratio between its width and height) is also considered in some studies (Tsinidis 2017, Tsinidis and Pitilakis 2018) from the literature. In this study, the aspect ratio is held constant at 1.0 (i.e., aspect ratio of a square) to have lesser number of combinations.

Table 1 Investigated parameter ranges

Parameter Name	Parameter Range
Depth ratio (R_D)	0.5, 1.0 and 1.5
Lateral distance ratio (R_L)	0, 2, and 4
Buried structure wall thickness (t_W)	0.50 m, 0.75 m and 1.00 m
Buried structure height (h)	5 m and 10 m
Surface structure fundamental period (T_B)	0.2, 0.4, 0.6, 0.8 and 1.0 sec
Peak amplitude of input motion acceleration (PGA)	0.10g, 0.30g and 0.50g

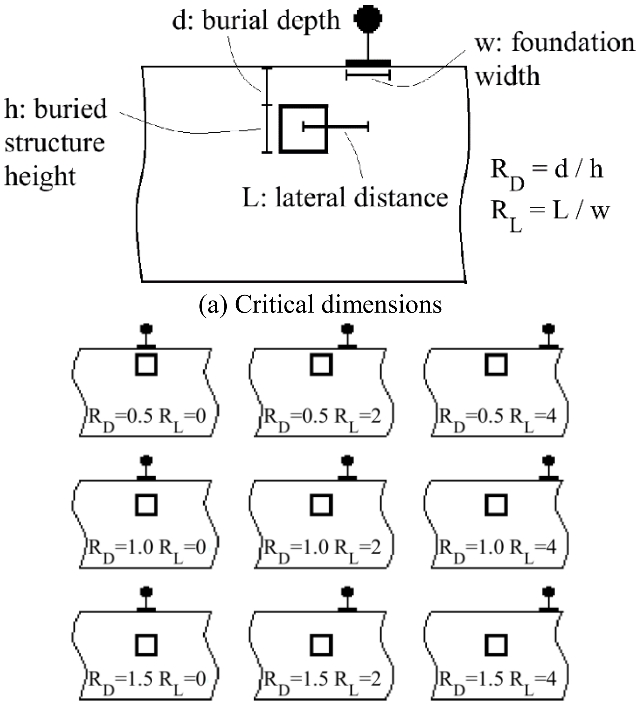

(b) Possible combinations of the depth ratio and the lateral distance ratio

Fig. 1 Critical dimensions and possible combinations of the depth ratio and the lateral distance ratio

The lateral distance ratio (R_L) parameter represents the ratio of the horizontal distance between the surface structure and the buried structure to the surface structure foundation width. In other words, the lateral distance ratio is a normalized measure of the distance between the surface structure and center of the buried structure. Foundation width and the lateral distance dimensions are given in Fig. 1. Also the possible combinations of the depth ratio and the lateral distance ratio are given in Fig. 1.

The surface structure is modelled in a way to have a raft foundation with a width of 16 m and a height of 1 m for all cases. The surface structure foundation is modelled so as to have a relatively rigid foundation and exclude the effects due to deformation of the foundation. The width value is selected so as to represent the width of a generic residential building. On the other hand, the mass of the foundation is accounted in the numerical models as distributed along the foundation width.

In the majority of the studies related to static and dynamic response of buried structures (Franza *et al*. 2017, Pitilakis *et al*. 2014, Tsinidis 2017, 2018, Tsinidis and Pitilakis 2018) a parameter named as flexibility ratio is considered. The flexibility ratio parameter corresponds to the ratio of diametric (for circular buried structures) or lateral (for rectangular buried structures) deformation stiffness of surrounding soil to that of the buried structure. In most of these studies, the variation of the flexibility ratio is generally assured by altering Young's Modulus of the buried structure material. However, in practice, Young's Modulus can only vary slightly for possible concrete materials. In fact, the variation of the flexibility ratio mainly corresponds to change in dimensions and wall cross-section of the buried structure (e.g., cross-section height contributes to buried structure stiffness with its cube). The change in the buried structure wall cross-section causes not only variation of the buried structure stiffness but also the variation of the buried structure mass. The inertial change in the buried structure is generally neglected in previous studies. There is only a limited number of studies (Sisman and Ayvaz 2019b, Xu *et al*. 2019) that account for variation of the buried structure mass. In this study, wall thickness and height of the buried structure are directly addressed to overcome possible inaccuracies due to omission of the mass variation effect.

The surface structure fundamental period (T_B) represents a dynamic characteristic of the surface structure. The surface structure fundamental period is also used as a parameter to control the number of stories of the surface structure. The number of stories and the fundamental period are correlated by using the approximation given here, T_B=0.1N, where T_B is in sec and N is the number of stories. The given approximate fundamental period equation is a well-known approximation used in practice. In this equation, T_B corresponds to the fundamental period and N represents the number of stories.

In the current study, the fundamental period of the surface structure can be equal to five different values. Those values are selected as given in Table 1 to represent low to high rise residential buildings. The surface structure is modelled as a single degree of freedom system (SDOF), i.e., mass and column system. The surface structure is modelled in a way to have 2, 4, 6, 8 and 10 stories, for periods of 0.2 sec, 0.4 sec, 0.6 sec, 0.8 sec and 1.0 sec, respectively. The corresponding surface structure masses are determined in accordance with current practice. Locations of the lumped SDOF masses are assumed to be at two-thirds of the total height of the surface structure (i.e., assuming triangular distribution of seismic forces along the height of the surface structure). The story height is assumed to be 3 m for all of the surface structures and the viscous damping ratio is assumed to be 5%. The corresponding lateral stiffness values are calculated in such a way to assure the predefined fundamental period values. The parameters used in modelling the surface structures are given in Table 2.

Table 2 SDOF system parameters

Fundamental period (sec)	SDOF mass (tons)	Effective height of the SDOF (m)
0.2	28.8	4
0.4	67.2	8
0.6	105.6	12
0.8	144.0	16
1.0	182.4	20

Mechanical behavior of soil deposits may be altered during stronger input motions due to the soil material nonlinearity. For this reason, a Ricker wavelet acceleration history is scaled to three different peak acceleration values to be used as input motions. The peak amplitude of input motion acceleration values given in Table 1 correspond to these three values. The Ricker wavelet amplitude (outcrop) is scaled to 0.10g, 0.30 g and 0.50 g in order to represent weak, moderate and strong earthquake input motions, respectively.

Finally, 810 different cases are generated for each soil site by considering combinations of the parameter values given in Table 1. On the other hand, cases excluding the buried structure are also generated, which are hereafter named as the free-field cases. Excluding the buried structure related parameters, there are only two parameters (i.e., surface structure fundamental period and peak amplitude of input motion acceleration) left. And possible 15 combinations can be generated for each soil site as the free-field cases. Thus, a total of 1650 times history analyses are conducted.

3. Numerical model

In this study, two-dimensional numerical models are generated by using OpenSEES (McKenna *et al*. 2010) software which utilizes Finite Element Method. Plane strain quadrilateral elements are used for modelling soil domain and frame elements are used for modelling both the surface structure and the buried structure. Since the numerical models are two-dimensional, the representative thickness is defined to be 1 m. Therefore, the buried structure wall stiffness and the surface structure mass values are calculated in such a way to represent 1 m length perpendicular to the two-dimensional plane.

In the numerical model, periodic boundary condition (PBC) is assigned to the lateral boundaries of the soil domain. The periodic boundary condition is a kind of boundary conditions which is generally utilized for approximating an infinitely long length by using a finite length. One dimensional (1D) wave propagation approaches assumes that the soil layers are infinitely long in horizontal direction. Thus, PBC can be used for finite element modelling of 1D wave propagation. The periodic type of boundary condition is achieved by enforcing the lateral

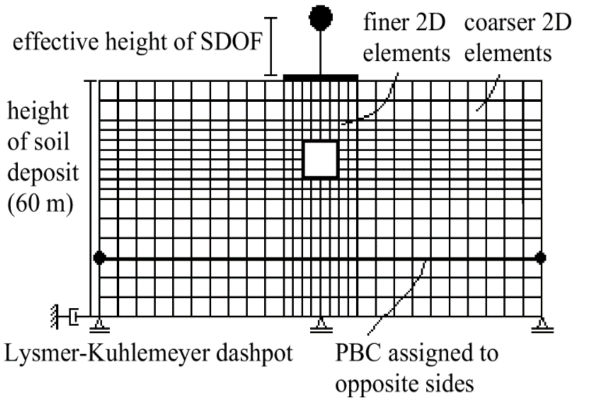

Fig. 2 Model sketch and representative mesh (not drawn according to scale)

Table 3 Soil mechanical properties

Property	Soil Site 1	Soil Site 2
Mass density (kg/m^3)	1.8	1.8
Poisson's ratio	0.25	0.25
Peak shear strain	0.10	0.10
Friction angle (°)	0	0
Cohesion (kPa)	20	40
Shear wave velocity (m/sec)	100	200

boundaries of the soil domain to move simultaneously (i.e. assigning equal degree of freedom in OpenSEES). One dimensional shear wave propagation is ensured by introducing the periodic boundary conditions. Besides, absorbing boundary conditions are also introduced at the base of the soil domain to assure radiation damping. For this purpose, a dash-pot element is attached to the base of the soil domain (Lysmer, J. and Kuhlemeyer 1969), as shown in Fig. 2. On the other hand, the input motion is applied as a force history to the base of the soil domain (Joyner and Chen 1975). The force history is calculated by using particle velocity history, i.e., velocity history of the input motion, at the base of the soil domain.

The soil domain width is determined to be 500 m by performing several preliminary convergence analyses. Two different element sizes are adopted for the quadrilateral elements, i.e. larger elements far from the structures and smaller elements in the vicinity of the structures (see Fig. 2). The largest element size adopted in this study is ensured to be smaller than 1/8 of the wavelength of the seismic wave with the maximum frequency of interest (~10 Hz). The time step in the numerical analyses is adopted in a way to ensure CFL condition (Courant *et al.* 1967) for wave propagation problems. The CFL condition, which stands for Courant–Friedrichs–Lewy, states that there must be a ratio between the numerical integration time step and the smallest mesh size for stability of numerical wave propagation analyses. According to this criterion, $C_S.\Delta t/u$ must be smaller than 1 where C_S is propagation velocity, Δt is the analysis time step and u is the smallest mesh size, in compatible units.

As stated before, the aim of this study is to investigate the dynamic surface structure-buried structure interactions in soft to moderate soil deposits. For this purpose, two single layer soil deposits with shear wave velocities of 100 m/sec and 200 m/sec are considered. The soil deposits have a height of 60 m each, and first fundamental period of the soil sites are 2.4 sec and 1.2 sec, respectively. For the soil deposits 5% viscous damping is employed, and the Rayleigh scheme is adopted to introduce both soil and structure damping ratios. The Pressure Independent Multi Yield material from the OpenSEES library is assigned to the quadrilateral elements which are representing the soil medium. The Pressure Independent Multi Yield material is appropriate for modelling organic soils or clay under fast (i.e., undrained) loading conditions (OpenSeesWiki, 2019). The deviatoric stress-strain behavior is elastic-plastic for the Pressure Independent Multi Yield material, while the volumetric stress-strain behavior is linear elastic. This material is suitable to model materials whose shear behavior is independent of the confinement pressure variation (i.e. Von Misses type of yield surfaces). The soil mechanical properties adopted in this study are given in Table 3. The stress-strain curve and the backbone curve obtained by using the given mechanical properties are given in Fig. 3 for both soil sites.

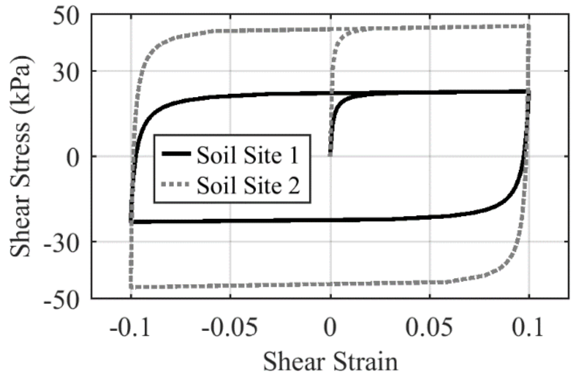

(a) Stress-strain curve

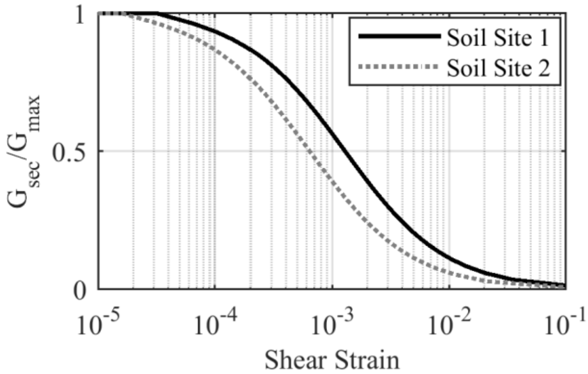

(b) Backbone curve

Fig. 3 Stress-strain behavior and backbone curves

Peak amplitudes of the input motions are mentioned in Table 1. The frequency content and time history of the input motion are given in Fig. 4. There are two reasons for employing Ricker wavelet acceleration histories instead of recorded earthquake histories. The first is to make the surface structure experience larger deformations, and the second is to exclude the input motion dependent results. To assure that the employed Ricker wavelet yields larger deformations than real earthquake recordings, displacement response spectra of some well-known seismic events are

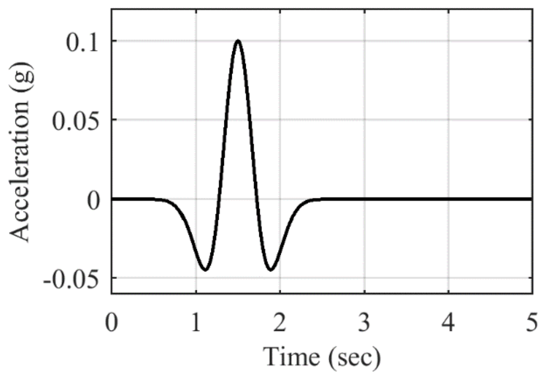

(a) Acceleration history

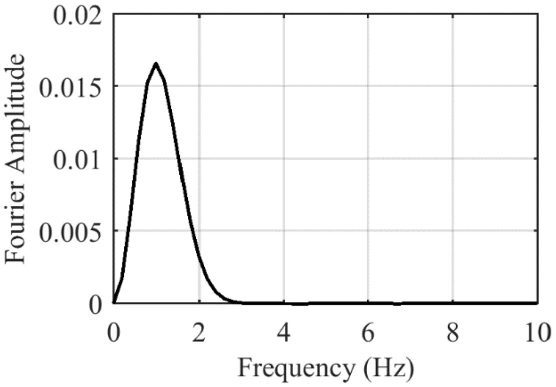

(b) Fourier Amplitude Spectrum

Fig. 4 Acceleration time history and FAS of the input motion (for 0.10g peak amplitude)

Table 4 Seismic events which are used for comparison

Event name	Station Name	Recorded at $V_{S,30}$ (m/sec)
Kobe, 1995	Kobe University	1043.00
Kobe, 1995	Nishi-Akashi	609.00
Kocaeli, 1999	Gebze	792.00
Northridge, 1994	LA Chalon Rd	740.05
Northridge, 1994	LA Wonderland Ave	1222.52

given in comparison with that of Ricker wavelet. Names and station properties of the real seismic events used for comparison are given in Table 4 (PEER Ground Motion Database, 2019). The displacement response spectra comparison is given in Fig. 5, and it is remarkable that Ricker wavelet yields larger spectral displacements. Since the employed Ricker wavelet is scaled to different peak amplitudes, its acceleration time history and Fourier Amplitude Spectrum (FAS) can be obtained by scaling the time history and FAS of the input motion with 0.10 g peak amplitude. Therefore, acceleration time history and FAS of the input motion with 0.10g peak amplitude are only given in Fig. 4.

The surface structure drifts and accelerations are utilized in this study to evaluate the interaction effects between the surface structure and the buried structure. As stated before, 15 free-field cases are modelled and corresponding responses (i.e., drifts and accelerations) are calculated for the surface structure for each soil site. The free-field surface structure responses for both soil sites are illustrated in Fig. 6

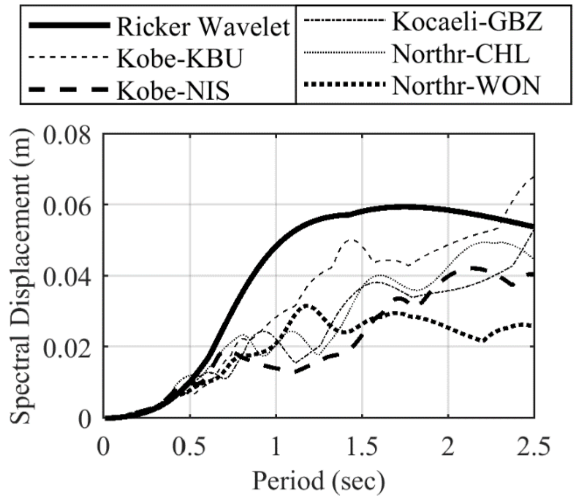

Fig. 5 Surface structure drift histories for Soil Site 1 in free-field conditions

and Fig. 7, respectively. Then, the surface structure responses for the 1620 different cases are determined by using the numerical models. Afterwards, the response amplification factor is defined as the ratio of the maximum response obtained in each case to the maximum response obtained in the corresponding free-field cases.

4. Results

After obtaining the surface structure drift and acceleration histories for Soil Site 1 and Soil Site 2, the variation of the surface structure response amplification factors with case parameters is illustrated. Fig. 8 to Fig. 11 show minimum, mean and maximum values of the response amplification factors for two different soil sites. The response amplification factors for each case are not explicitly given due to space limitations. Each of the four figures (i.e., Fig. 8 to Fig. 11), is composed of six different graphs. These six graphs correspond to six case parameters which are wall thickness of buried structure (i.e., t_W), lateral distance ratio (i.e., R_L), depth ratio (i.e., R_D), buried structure height (i.e., h), input motion PGA (i.e., PGA) and fundamental period of surface structure (T_B). Each graph consists of three different illustrations representing minimum, mean and maximum of the response amplification factors.

Prior to evaluation of effect of the case parameters on the surface structure responses, a brief explanation of the mechanisms behind the response variations is given here.

The buried structure located inside a soil deposit can be thought as a fictitious soil layer inside the soil deposit. In this case, the fictitious soil layer would have the same lateral stiffness and mass density (i.e. the same dynamic impedance) with the buried structure. On the other hand, the surface structure and its foundation system can be thought as another fictitious soil layer (Safak 1999). The impedance ratios among the actual soil layer and these two fictitious soil layers are key to the response variations.

Beyond the impedance ratios, presence of a lumped

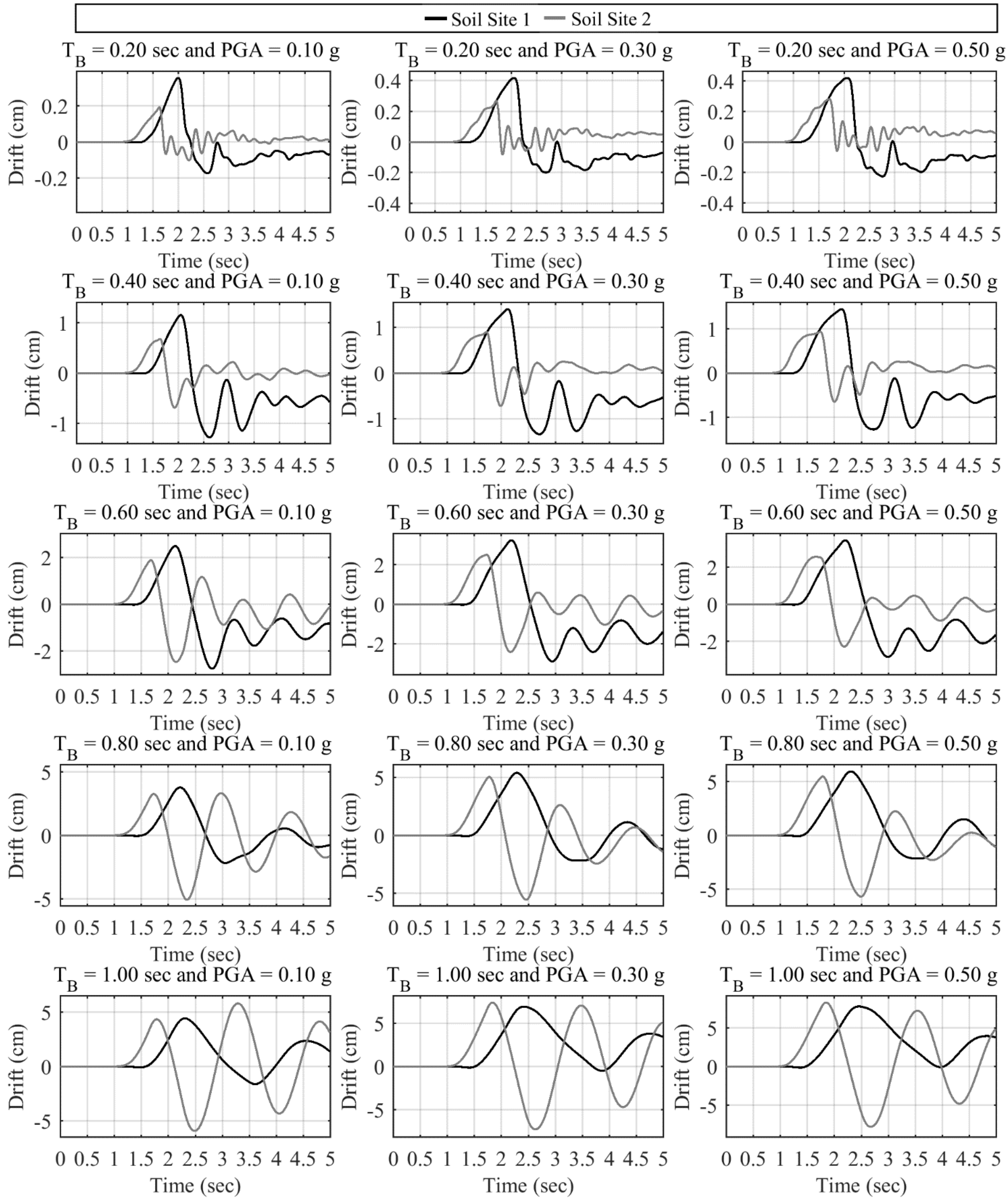

Fig. 6 Surface structure drift histories for Soil Site 1 and Soil Site 2 in free-field conditions

mass inside a continuous medium causes scattering of the propagating waves (Doyle 1989). Thus, depending on the amount of located mass and the medium characteristics, the surface structure responses vary.

The soil nonlinearity is another important phenomenon which is effective on the surface structure responses. High level of soil nonlinearity results in high level of hysteretic energy dissipation. The seismic input energy reaching to the ground surface varies with varying level of soil nonlinearity. Thus, the surface structure responses vary with the level of soil nonlinearity.

As stated above, the surface structure can be considered as a fictitious soil layer. Depending on the impedance ratio between the surface structure and the soil layer the amount

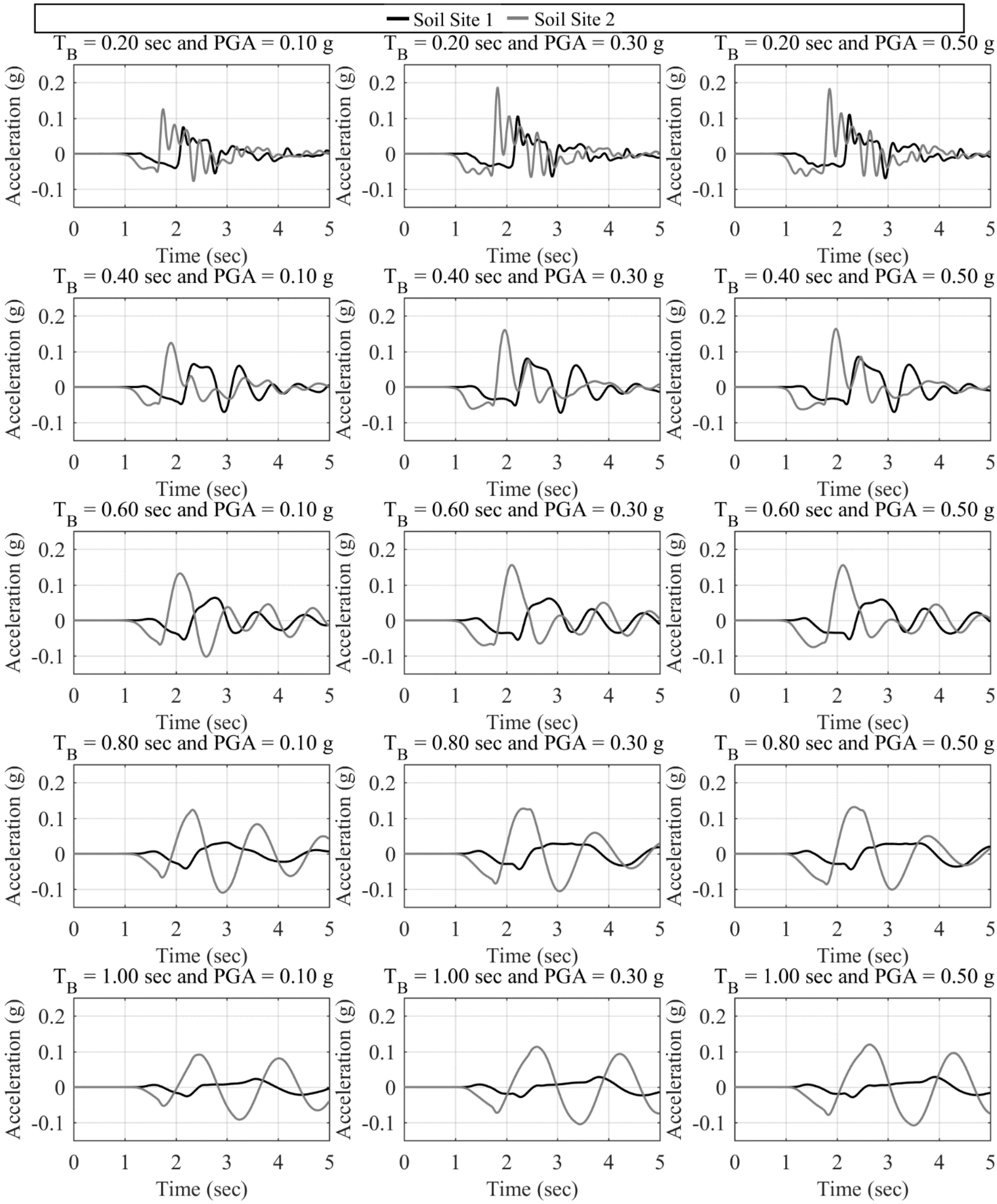

Fig. 7 Surface structure acceleration histories for Soil Site 1 and Soil Site 2 in free-field conditions

of radiation damping varies. The additional damping results in variations of the surface structure responses. Besides, it causes different variation patterns for drift responses and acceleration responses (i.e., when the drifts are amplified the accelerations may be de-amplified). As it is known from the dynamics of the structures theory, the peak drift values are proportional to the peak acceleration values (i.e., ω^2. SD=PSA and PSA≈SA, where ω: radial frequency, SD: spectral displacement, PSA: Pseudo Spectral Acceleration and SA: Spectral Acceleration) in case of lower damping ratios. Addition of high level of radiation damping to the dynamic systems breaks down this proportionality.

It is shown in the literature that the buried structures

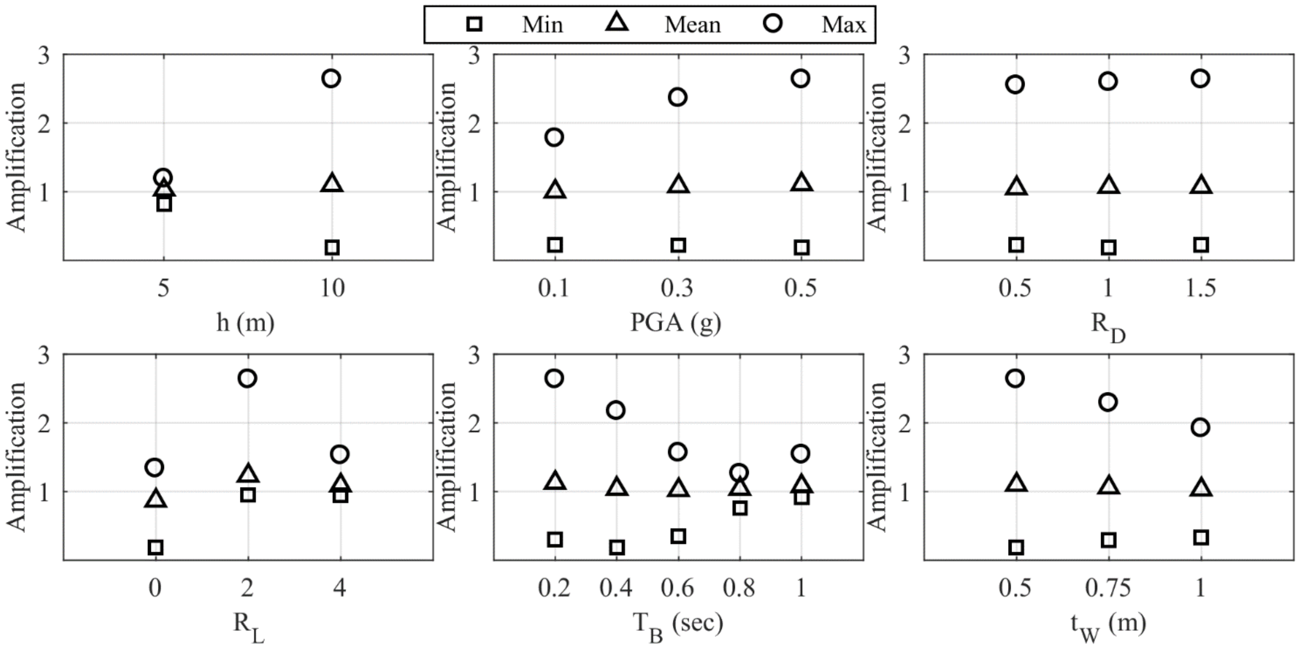

Fig. 8 Variation of the surface structure drift amplification factors with case parameters for Soil Site 1

create a ‘shadow zone’ (Yiouta-Mitra *et al*. 2007) on the ground surface for the propagating shear waves. Namely, if a surface structure is located on the shadow zone, response of the structure generally decreases. It is similar to the propagation paths of the body waves through the earth’s mantle. The shear waves cannot propagate through the outer core which is in liquid form and this creates a shadow zone on the earth’s crust.

As stated before, locating a lumped mass inside a continuous medium causes scattering of the propagating waves. The scattered waves then concentrate at the ground surface. However, the concentration level varies for different lateral distances from the lumped mass (i.e., buried structure) location. Thus, the surface structure responses vary with their lateral distance to the buried structure.

As stated above, the buried structure located inside a soil deposit can be thought as a fictitious soil layer inside the soil deposit. Due to the impedance difference between the actual soil layer and the fictitious one, shear waves can be trapped between these two layers. And depending on height of the trapping zone, frequency characteristics of the trapped waves vary. Thus, the surface structures with different frequency characteristics yield different response variations.

4.1 Drift amplifications

The findings related to variation of the drift amplifications/de-amplifications with each case parameter (i.e., h, PGA, R_D, t_W, R_L and T_B) are given in an independent paragraph below to assure reading convenience.

As seen from the figures Figs. 8 and 9, the drift amplification factors for the Soil Site 1 are higher than the drift amplification factors for Soil Site 2. For Soil Site 1, the maximum drift amplification factor is 2.64, which translates to 164% amplification of the surface structure drifts. For the same soil conditions, the minimum surface structure drift amplification factor is 0.19, which means 81% de-amplification of the surface structure drifts. On the other hand, for the Soil Site 2, the maximum drift amplification factor is 1.65, which means 65% amplification of the surface structure drifts. For the same soil conditions, the minimum amplification factor is 0.32, which corresponds to 68% de-amplification of the surface structure drifts. As given before, these two soil sites have different mechanical properties, which yields different dynamic impedances as well as different nonlinearity levels. Besides, the amount of radiation damping also changes due to the variation of the soil mechanical properties. The variations in these three phenomena (i.e., the impedance ratios, the soil nonlinearity and the amount of radiation damping) results in varying amplification/de-amplification percentages.

As seen from the figures Figs. 8 and 9, the drift amplification factors for both soil sites deviate from 1 for increasing buried structure height (i.e., h) values. For the cases where h=5 m, the maximum drift amplification factor is 1.19, which means 19% amplification of the surface structure drifts. For the same cases the minimum amplification factor is 0.83, which means 17% de-amplification of the surface structure drifts. For the cases where h=10 m, the maximum drift amplification factor is 2.64, which means 164% amplification of the surface structure drifts. For the same cases the minimum amplification factor is 0.19, which means 81% de-amplification of the surface structure drifts. Increasing the buried structure height (i.e., h) decreases the lateral distortion stiffness and the impedance ratio between the soil layer and the buried structure changes. On the other hand, the amount of the lumped mass located inside the soil deposit increases with increasing buried structure height. The variations in these two phenomena (i.e., the impedance

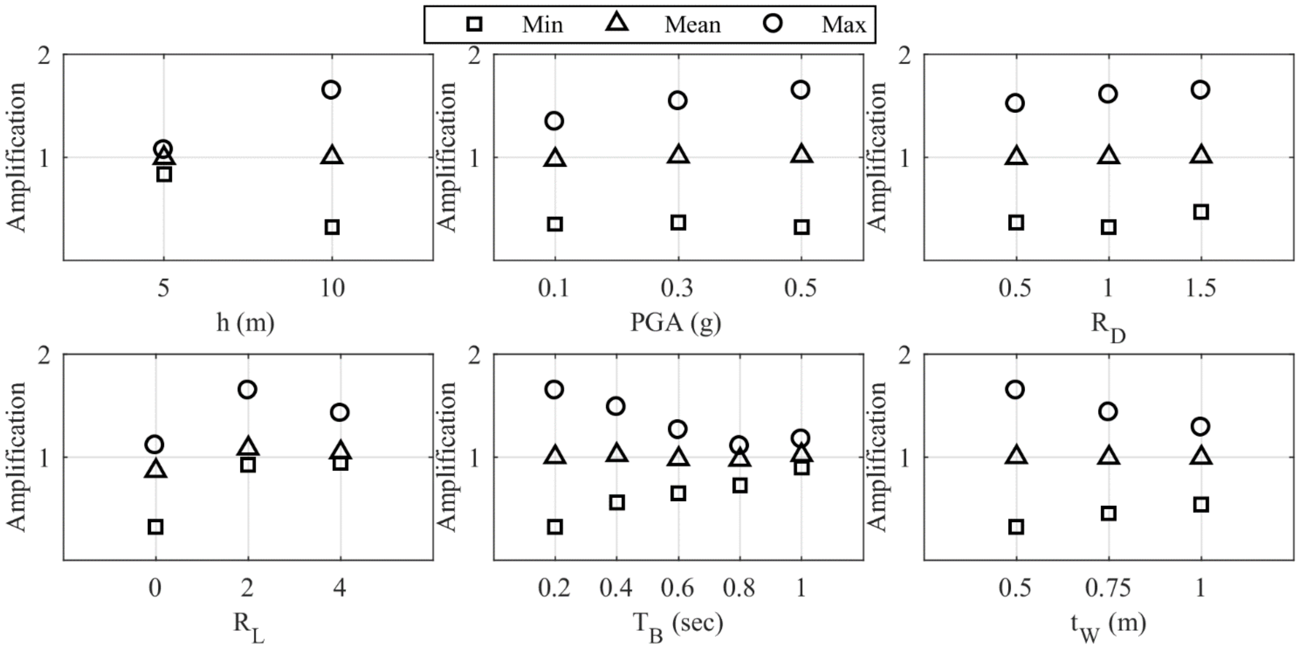

Fig. 9 Variation of the surface structure drift amplification factors with case parameters for Soil Site 2

ratios and the located lumped mass) results in varying amplification/de-amplification percentages.

As seen from the figures Figs. 8 and 9, the drift amplification factors for both soil sites increase with increasing input motion PGA values. For the cases where PGA is 0.10 g, the maximum drift amplification factor is 1.78, which is equal to 78% amplification of the surface structure drifts. For the same cases the minimum amplification factor is 0.23, which means 77% de-amplification of the surface structure drifts. For the cases where PGA is 0.30g, the maximum drift amplification factor is 2.36, which means 136% amplification of the surface structure drifts. For the same cases the minimum amplification factor is 0.22, which means 78% de-amplification of the surface structure drifts. For the cases where PGA is 0.50 g, the maximum drift amplification factor is 2.64, which means 164% amplification of the surface structure drifts. For the same cases the minimum amplification factor is 0.19, which means 81% de-amplification of the surface structure drifts. As the input motion PGA varies the level of soil nonlinearity varies. Since the soil stiffness changes with the input motion PGA level, the impedance of the soil deposit is also varying. The variations in these two phenomena (i.e., the impedance ratios and the soil nonlinearity) results in varying amplification/de-amplification percentages.

As seen from the figures Figs. 8 and 9, the drift amplification factors for both soil sites increase with increasing depth ratio (i.e., R_D) values. For the cases where R_D=0.5, the maximum drift amplification factor is 2.55, which means 155% amplification of the surface structure drifts. For the same cases the minimum amplification factor is 0.23, which means 77% de-amplification of the surface structure drifts. For the cases where R_D=1.0, the maximum drift amplification factor is 2.59, which means 159% amplification of the surface structure drifts. For the same cases the minimum amplification factor is 0.19, which means 81% de-amplification of the surface structure drifts. For the cases where R_D=1.5, the maximum drift amplification factor is 2.64, which means 164% amplification of the surface structure drifts. For the same cases the minimum amplification factor is 0.23, which means 77% de-amplification of the surface structure drifts. As the depth ratio varies height of the trapping zone varies. The variations in the trapping zone phenomenon results in varying amplification/de-amplification percentages.

As seen from the figures Fig. 8, the drift amplification factors for both soil sites decrease with increasing buried structure wall thickness (i.e., t_W) values. For the cases where t_W=0.50 m, the maximum drift amplification factor is 2.64, which means 164% amplification of the surface structure drifts. For the same cases the minimum amplification factor is 0.19, which means 81% de-amplification of the surface structure drifts. For the cases where t_W=0.75 m, the maximum drift amplification factor is 2.29, which means 129% amplification of the surface structure drifts. For the same cases the minimum amplification factor is 0.30, which means 70% de-amplification of the surface structure drifts. For the cases where t_W=1.00 m, the maximum drift amplification factor is 1.92, which means 92% amplification of the surface structure drifts. For the same cases the minimum amplification factor is 0.33, which means 67% de-amplification of the surface structure drifts. Increasing the buried structure wall thickness (i.e., t_W) increases the lateral distortion stiffness, and the impedance ratio between the soil layer and the buried structure changes. On the other hand, the amount of the lumped mass located inside the soil deposit increases with increasing buried structure wall thickness. The variations in these two phenomena (i.e., the impedance ratios and the located lumped mass) results in varying amplification/de-amplification percentages.

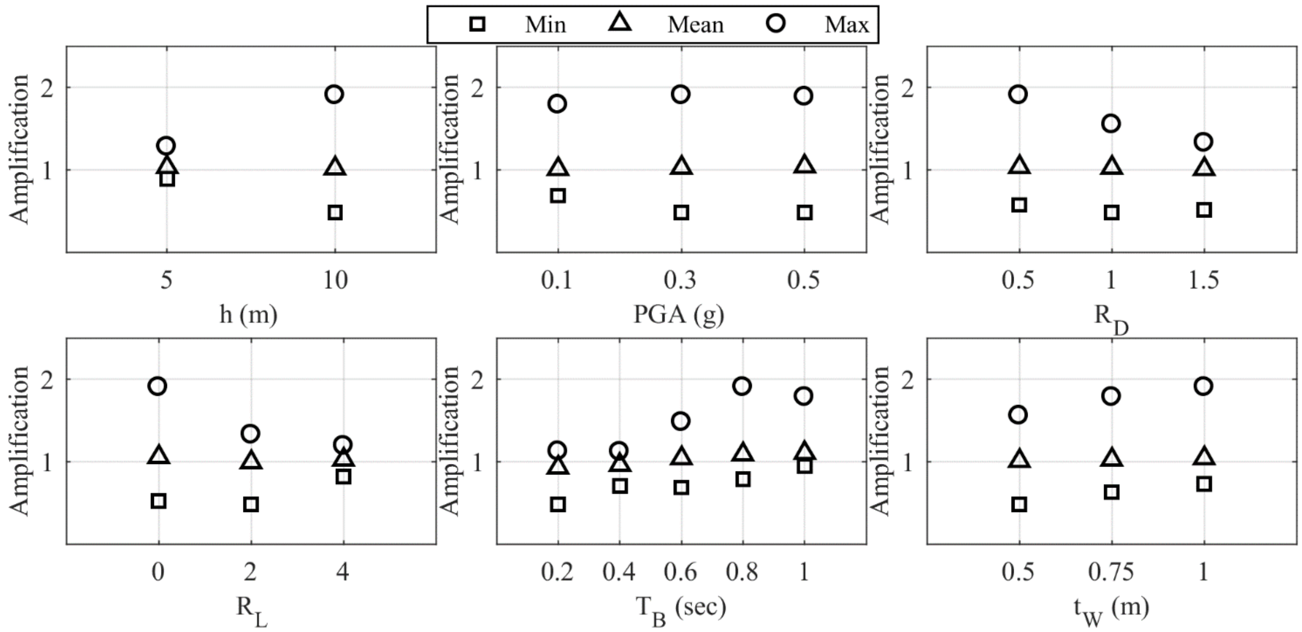

Fig. 10 Variation of the surface structure acceleration amplification factors with case parameters for Soil Site 1

As seen from the figures Figs. 8 and 9, variation of the drift amplification factors with the lateral distance ratio parameter (i.e., R_L) is a bit complex. For the cases where R_L=0, the minimum surface structure drift amplification factor is 0.19, which means 81% de-amplification of the surface structure drifts. For the same cases (i.e., R_L=0) the maximum surface structure drift amplification factor is 1.34, which means 34% amplification of the surface structure drifts. For the cases where R_L=2, the maximum surface structure drift amplification factor is 2.64, which means 164% amplification of the surface structure drifts. For the same cases (i.e., R_L=2) the minimum surface structure drift amplification factor is 0.93, which means only 7% de-amplification of the surface structure drifts. For the cases where R_L=4, the maximum surface structure drift amplification factor is 1.53, which means 53% amplification of the surface structure drifts. For the same cases (i.e., R_L=4) the minimum surface structure drift amplification factor is 0.94, which means only 6% de-amplification of the surface structure drifts. The R_L=0 corresponds to the surface structure to be located on the shadow zone. On the other hand, the other two R_L values corresponds to different concentration levels of the scattered waves. Occurrence of these two phenomena (i.e. the shadow zone and the scattered wave concentration) results in varying amplification/de-amplification percentages.

Also, it can be seen in Fig. 8 and Fig. 9, the variation of the drift amplification factors with the surface structure fundamental period (i.e., T_B) is quite complex. For the cases where T_B=0.2 sec, the maximum surface structure amplification factor is 2.64, which means 164% amplification of the surface structure drifts. For the same cases the minimum amplification factor is 0.31, which means 69% de-amplification of the surface structure drifts. For the cases where T_B=0.4 sec, the maximum surface structure amplification factor is 2.17, which means 117% amplification of the surface structure drifts. For the same cases the minimum amplification factor is 0.19, which means 81% de-amplification of the surface structure drifts. For the cases where T_B=0.6 sec, the maximum surface structure amplification factor is 1.56, which means 56% amplification of the surface structure drifts. For the same cases the minimum amplification factor is 0.35, which means 65% de-amplification of the surface structure drifts. For the cases where T_B=0.8 sec, the maximum surface structure amplification factor is 1.26, which means 26% amplification of the surface structure drifts. For the same cases the minimum amplification factor is 0.73, which means 27% de-amplification of the surface structure drifts. For the cases where T_B=1.0 sec, the maximum surface structure amplification factor is 1.54, which means 54% amplification of the surface structure drifts. For the same cases the minimum amplification factor is 0.90, which means 10% de-amplification of the surface structure drifts. Increasing the surface structure fundamental period (i.e., T_B) decreases the SDOF stiffness and increases the SDOF mass, and the impedance ratio between the soil layer and the surface structure changes. On the other hand, depending on this impedance ratio, the amount of radiation damping changes. The variations in these two phenomena (i.e., the impedance ratios and the amount of radiation damping) results in varying amplification/de-amplification percentages.

4.2 Acceleration amplifications

The findings related to the acceleration amplification/de-amplifications for each case parameter (i.e., h, PGA, R_D, t_W, R_L and T_B) are given in an independent paragraph below to assure reading convenience.

As seen from Figs. 10 and 11, the acceleration amplification factors for the Soil Site 1 are higher than the

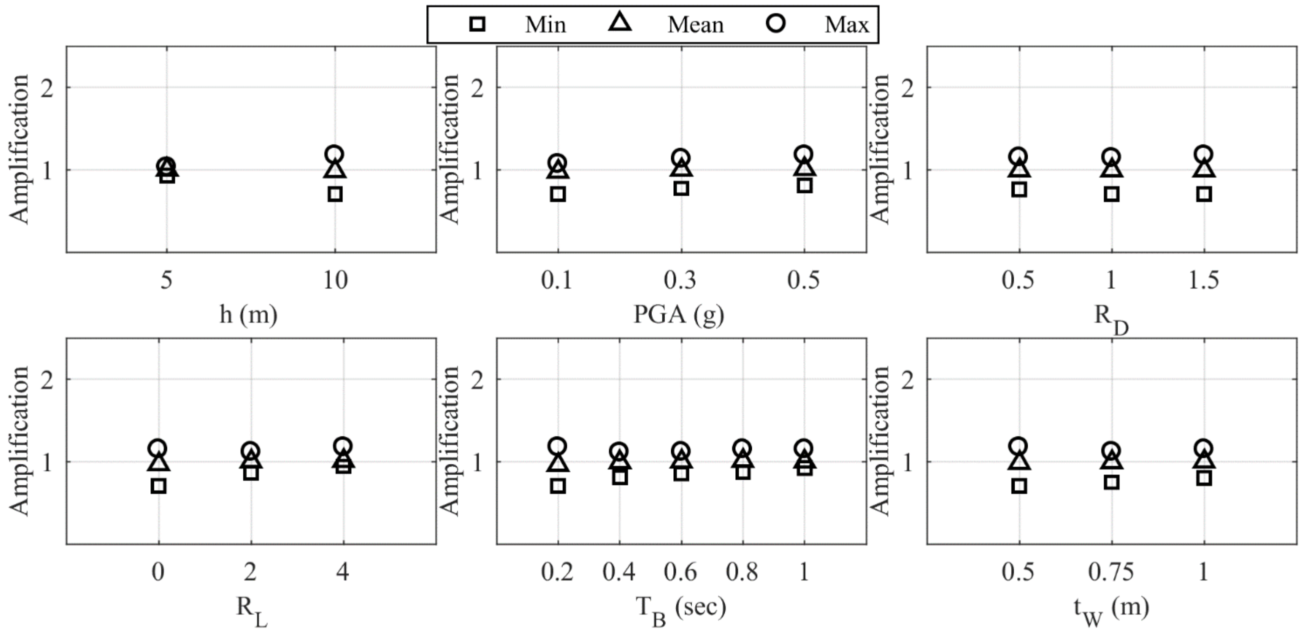

Fig. 11 Variation of the surface structure acceleration amplification factors with case parameters for Soil Site 2

acceleration amplification factors for Soil Site 2. For Soil Site 1, the maximum acceleration amplification factor is 1.91, which means 91% amplification of the surface structure accelerations. For the same soil conditions, the minimum surface structure acceleration amplification factor is 0.49, which means 51% de-amplification of the surface structure accelerations. On the other hand, for the Soil Site 2, the maximum acceleration amplification factor is 1.18, which means 18% amplification of the surface structure accelerations. For the same soil conditions, the minimum amplification factor is 0.71, which corresponds to 29% de-amplification of the surface structure accelerations. As it was the case for the surface structure drifts, these two soil sites have different mechanical properties, which yields different dynamic impedances as well as different nonlinearity levels. Besides, the amount of radiation damping also changes due to the variation of the soil mechanical properties. The variations in these three phenomena (i.e. the impedance ratios, the soil nonlinearity and the amount of radiation damping) results in varying amplification/de-amplification percentages. Besides, existence of the radiation damping yields different amplification/de-amplification patterns for acceleration responses when compared to the drift responses.

As seen from the figures Figs. 10 and 11, the acceleration amplification factors for both soil sites increase with increasing buried structure height (i.e. h) values. For the cases where h=5 m, the maximum acceleration amplification factor is 1.28, which means 28% amplification of the surface structure accelerations. For the same cases the minimum amplification factor is 0.90, which means 10% de-amplification of the surface structure accelerations. For the cases where h=10 m, the maximum acceleration amplification factor is 1.91, which means 91% amplification of the surface structure accelerations. For the same cases the minimum amplification factor is 0.49, which means 51% de-amplification of the surface structure accelerations. As it was the case for the surface structure drifts, increasing the buried structure height (i.e., h) decreases the lateral distortion stiffness and the impedance ratio between the soil layer and the buried structure changes. On the other hand, the amount of the lumped mass located inside the soil deposit increases with increasing buried structure height. The variations in these two phenomena (i.e., the impedance ratios and the located lumped mass) results in varying amplification/de-amplification percentages. Besides, existence of the radiation damping yields different amplification/de-amplification patterns for acceleration responses when compared to the drift responses.

As seen from the figures Figs. 10 and 11, the acceleration amplification factors for both soil sites generally increase with increasing input motion PGA values. For the cases where PGA is 0.10g, the maximum acceleration amplification factor is 1.79, which means 79% amplification of the surface structure accelerations. For the same cases the minimum amplification factor is 0.69, which means 31% de-amplification of the surface structure accelerations. For the cases where PGA is 0.30 g, the maximum acceleration amplification factor is 1.91, which means 91% amplification of the surface structure accelerations. For the same cases the minimum amplification factor is 0.49, which means 51% de-amplification of the surface structure accelerations. For the cases where PGA is 0.50 g, the maximum acceleration amplification factor is 1.89, which means 89% amplification of the surface structure accelerations. For the same cases the minimum amplification factor is 0.49, which means 51% de-amplification of the surface structure accelerations. As it was the case for the surface structure drifts, as the input motion PGA varies the level of soil nonlinearity varies. Since the soil stiffness changes with the input motion PGA level, the impedance of the soil deposit also varies. The variations in these two phenomena (i.e., the

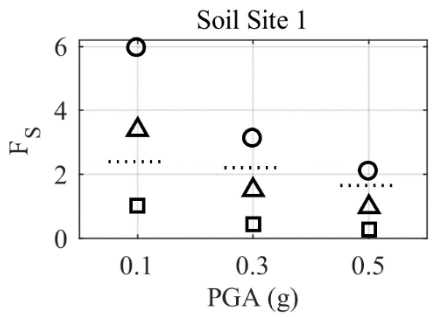

(a) F_S for Soil Site 1

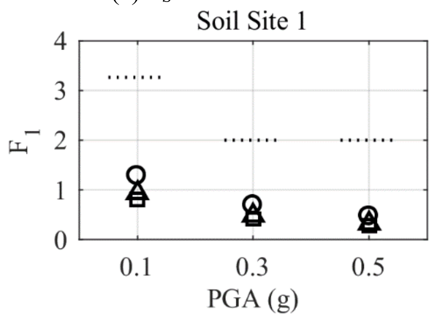

(b) F_1 for Soil Site 1

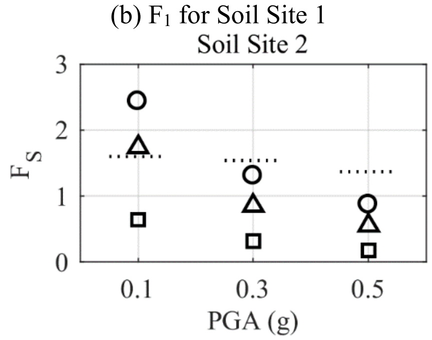

(c) F_S for Soil Site 2

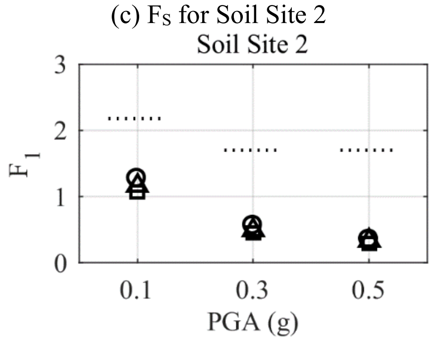

(d) F_1 for Soil Site 2

Fig. 12 Variation of soil amplification coefficients

impedance ratios and the soil nonlinearity) results in varying amplification/de-amplification percentages. Besides, existence of the radiation damping yields different amplification/de-amplification patterns for acceleration responses when compared to the drift responses.

As seen from the figures Figs. 10 and 11, the acceleration amplification factors for both soil sites generally decrease with increasing depth ratio (i.e., R_D) values. For the cases where R_D=0.5, the maximum acceleration amplification factor is 1.91, which means 91% amplification of the surface structure accelerations. For the same cases the minimum amplification factor is 0.58, which means 42% de-amplification of the surface structure accelerations. For the cases where R_D=1.0, the maximum acceleration amplification factor is 1.55, which means 55% amplification of the surface structure accelerations. For the same cases the minimum amplification factor is 0.49, which means 51% de-amplification of the surface structure accelerations. For the cases where R_D=1.5, the maximum acceleration amplification factor is 1.33, which means 33% amplification of the surface structure accelerations. For the same cases the minimum amplification factor is 0.52, which means 48% de-amplification of the surface structure accelerations. As it was the case for the surface structure drifts, as the depth ratio varies, height of the trapping zone varies. The variations in the trapping zone phenomenon results in varying amplification/de-amplification percentages. Besides, existence of the radiation damping yields different amplification/de-amplification patterns for acceleration responses when compared to the drift responses.

As seen from the figures Figs. 10 and 11, the acceleration amplification factors for both soil sites generally increase with increasing buried structure wall thickness (i.e., t_W) values. For the cases where t_W=0.50 m, the maximum acceleration amplification factor is 1.56, which means 56% amplification of the surface structure accelerations. For the same cases the minimum amplification factor is 0.49, which means 51% de-amplification of the surface structure accelerations. For the cases where t_W=0.75 m, the maximum acceleration amplification factor is 1.79, which means 79% amplification of the surface structure accelerations. For the same cases the minimum amplification factor is 0.63, which means 37% de-amplification of the surface structure accelerations. For the cases where t_W=1.00 m, the maximum acceleration amplification factor is 1.91, which means 91% amplification of the surface structure accelerations. For the same cases the minimum amplification factor is 0.74, which means 26% de-amplification of the surface structure accelerations. As it was the case for the surface structure drifts, increasing the buried structure wall thickness (i.e., t_W) increases the lateral distortion stiffness, and the impedance ratio between the soil layer and the buried structure changes. On the other hand, the amount of the lumped mass located inside the soil deposit increases with increasing buried structure wall thickness. The variations in these two phenomena (i.e., the impedance ratios and the located lumped mass) results in varying amplification/de-amplification percentages. Besides, existence of the radiation damping yields different amplification/de-amplification patterns for acceleration responses when compared to the drift responses.

As seen from the figures Figs. 10 and 11, variation of the acceleration amplification factors with the lateral distance ratio parameter (i.e., R_L) is a bit complex. For the cases where R_L=0, the minimum surface structure acceleration amplification factor is 0.52, which means 48% de-amplification of the surface structure accelerations. For the same cases (i.e., R_L=0) the maximum surface structure acceleration amplification factor is 1.91, which means 91% amplification of the surface structure accelerations. For the cases where R_L=2, the maximum surface structure acceleration amplification factor is 1.33, which means 33% amplification of the surface structure accelerations. For the same cases (i.e., R_L=2) the minimum surface structure acceleration amplification factor is 0.49, which means 51% de-amplification of the surface structure accelerations. For the cases where R_L=4, the maximum surface structure acceleration amplification factor is 1.19, which means 19% amplification of the surface structure accelerations. For the same cases (i.e., R_L=4) the minimum surface structure acceleration amplification factor is 0.82, which means 18% de-amplification of the surface structure accelerations. As it was the case for the surface structure drifts, the R_L=0 corresponds to the surface structure to be located on the shadow zone. On the other hand, the other two R_L values corresponds to different concentration levels of the scattered waves. Occurrence of these two phenomena (i.e., the shadow zone and the scattered wave concentration) results in varying amplification/de-amplification percentages. Besides, existence of the radiation damping yields different amplification/de-amplification patterns for acceleration responses when compared to the drift responses.

As seen from the figures Figs. 10 and 11, variation of the acceleration amplification factors with the surface structure fundamental period (i.e., T_B) is quite complex. For the cases where T_B=0.2 sec, the maximum surface structure amplification factor is 1.18, which means 18% amplification of the surface structure accelerations. For the same cases the minimum amplification factor is 0.49, which means 51% de-amplification of the surface structure accelerations. For the cases where T_B=0.4 sec, the maximum surface structure amplification factor is 1.12, which means 12% amplification of the surface structure accelerations. For the same cases the minimum amplification factor is 0.71, which means 29% de-amplification of the surface structure accelerations. For the cases where T_B=0.6 sec, the maximum surface structure amplification factor is 1.49, which means 49% amplification of the surface structure accelerations. For the same cases the minimum amplification factor is 0.69, which means 31% de-amplification of the surface structure accelerations. For the cases where T_B=0.8 sec, the maximum surface structure amplification factor is 1.91, which means 91% amplification of the surface structure accelerations. For the same cases the minimum amplification factor is 0.79, which means 21% de-amplification of the surface structure accelerations. For the cases where T_B=1.0 sec, the maximum surface structure amplification factor is 1.79, which means 21% amplification of the surface structure accelerations. For the same cases the minimum amplification factor is 0.93, which means 7% de-amplification of the surface structure accelerations. As it was the case for the surface structure drifts, increasing the surface structure fundamental period (i.e., T_B) decreases the SDOF stiffness and increases the SDOF mass, and the impedance ratio between the soil layer and the surface structure changes. On the other hand, depending on this impedance ratio, the amount of radiation damping changes. The variations in these two phenomena (i.e., the impedance ratios and the amount of radiation damping) results in varying amplification/de-amplification percentages. Besides, existence of the radiation damping yields different amplification/de-amplification patterns for acceleration responses when compared to the drift responses.

4.3 Contribution to the subject

The current seismic design specification in Turkey (i.e., Turkish Building Earthquake Code, TBEC 2018) presents two soil amplification factors (F_S and F_1) for five different soil classes to be used for determination of elastic design spectrum.

The coefficient F_S corresponds to the short period (T=0.2 sec) soil amplification factor, and F_1 corresponds to the long period (T=1.0 sec) soil amplification factor. These coefficients simply represent the ratio of the acceleration responses on the soil surface to the acceleration responses on outcropping rock surface.

The case combinations of the study include surface structures with fundamental periods of both 0.2 sec and 1.0 sec. By dividing the peak acceleration responses of these two structures to the corresponding spectral accelerations calculated for outcropping rock motion, F_S and F_1 coefficients can be determined. The corresponding F_S and F_1 values provided in TBEC2018 are also determined for comparison. The minimum, the mean and the maximum values of the amplification coefficients calculated for all the cases are illustrated in Fig. 12. There are four graphs on Fig. 12 which corresponds to possible combinations of two soil sites (i.e., Soil Site 1 and Soil Site 2) and the two types of coefficients (i.e., F_S and F_1). In all four graphs, the corresponding F_S and F_1 values provided by TBEC 2018 are also depicted. In this study, the surface structure is directly modelled as a SDOF system in the FEM models and soil structure interaction is more comprehensively accounted for. Thus, the obtained values of F_S and F_1 coefficients are well above those provided by the code. Hence, it is natural to obtain an imperfect fit between the calculated coefficients and the code provided ones.

As seen from Fig. 12, the coefficient F_S has larger values than F_1 in contrast with TBEC 2018. In TBEC 2018, the provided F_1 values are generally larger than the F_S values. As stated before, in this study the input motion has a fundamental period of 1.0 sec, which means larger amplitudes at 1.0 sec period. On the other hand, larger amplitudes cause larger hysteretic energy dissipation due to the soil nonlinearity. Thus, the soil amplification coefficients corresponding to 1.0 sec (i.e., F_1) becomes smaller. Similarly, the F_1 values are always below the TBEC 2018 provided values. This is also because of the high level of hysteretic energy dissipation due to the soil nonlinearity. Beyond that, the hysteretic energy dissipation increases with larger input motion PGA values, and results in smaller F_1 and F_S values, as shown in Fig. 12.

The coefficient F_S has more scattered values than the coefficient F_1, which indicates that F_S is more sensitive to the case parameters mentioned previously. The F_S values gets smaller than the values provided in TBEC 2018 as the input motion PGA increases, and the scattering of the values diminishes. It seems that, increasing level of hysteretic energy dissipation dominates the other mechanisms which are effective on the response of the soil deposits. This is also why the F_I values are not scattered as much as F_S values.

Comparison of the F_S values for different soil sites is a bit complicated. It is a fact that, smaller soil stiffness causes higher soil amplifications in linear elastic soil conditions. However, when soil nonlinearity is included this fact can be reversed. For the F_S coefficient it can be said that Soil Site 1 (i.e., softer than Soil Site 2) yields larger values. Since the response amplitude corresponding to the short period is smaller, stress-strain behavior of the soil sites gets closer to the linear elastic behavior. Thus, the analyses yield larger F_S values. On the other hand, for the F_1 coefficient it can be said that Soil Site 2 yields slightly larger values. This is directly related with the level of the hysteretic energy dissipation. As the soil site gets stiffer, i.e., nonlinearity decreases, the dissipated hysteretic energy decreases. Thus, the F_1 values are larger for Soil Site 2.

In conclusion, it is apparent that the F_S and F_1 values provided by TBEC 2018 are generally more conservative. Due to the specificity of the input motion utilized in this study, a general inference cannot be made. However, this study gives insight about the phenomena and encourages further studies.

In the recent seismic code of Turkey (i.e., TBEC 2018), there is parameter named as spectral displacement ratio (i.e., C_R) to determine the inelastic spectral displacement demand by using the elastic one. Simply, the inelastic spectral displacement demand is equal to the product of C_R and the elastic spectral displacement demand. Similar coefficients can be found in the literature (Uang and Maarouf 1994) and are generally named as deflection amplification factors (DAF). The typical values for DAF can be roughly estimated to be between 1 and 5. There are a number of studies (Rizwan *et al.* 2019) which presents the DAF values for varying system properties. It is important to note that the reported DAF values are quite over 5. As stated before, the inelastic spectral displacement demand of a structure can be calculated by using the DAF value and the elastic spectral displacement demand. Then, the inelastic spectral displacement demand can be compared with the inelastic displacement capacity (Ahmad *et al.* 2012, Ahmad *et al.* 2017).

The drift amplification factors calculated in this study show that the elastic spectral displacement demand should be revised in case the structure is located in the vicinity of a buried structure. As given above, in the most critical case, the surface structure drifts can be amplified approximately 3 times. Thus, there is a need emerges for another coefficient besides the DAF. This coefficient corresponds the interaction amplification factor (IAF) due to the existence of a buried structure. The jointly use of the DAF and the IAF will provide safer seismic design of the buildings. However, practical IAF values are left for future studies.

5. Conclusions

A large number of two-dimensional numerical models are generated for dynamic time history analyses of a soil deposit with a surface structure and a buried structure. The dynamic interaction phenomenon between the surface structure and the buried structure is investigated by obtaining surface structure drift and acceleration amplifications for six different parameters including geometrical configuration of the structures, peak amplitudes of the input motions and fundamental period of the surface structure. The conclusions inferred from the response amplification illustrations are listed as;

(i) As the lateral distortion stiffness (i.e. decrease of h or increase of t_W) of the buried structure increases, both the drift and the acceleration amplification factors converge to 1. However, for the acceleration amplification factors this pattern is not as remarkable as it was for the drift amplification factors.

(ii) The surface structure drift and acceleration amplification factors generally increase for the larger values of the peak amplitude of the input motion. However, this variation is not remarkable for most of the cases.

(iii) The surface structure drift and acceleration amplification factors are generally non-sensitive to the depth ratio parameter (R_D). However, the surface structure drift amplification factors are very sensitive to the lateral distance ratio parameter (R_L). The cases where R_L=0 causes de-amplification of the surface structure drifts while the cases where R_L=2 and R_L=4 cause amplification of the surface structure drifts. On the other hand, the acceleration amplification factors generally converge to 1 as the parameter R_L increases.

(iv) The low to mid rise buildings experience much more drift amplifications/de-amplifications than the high-rise buildings. Similarly, the acceleration amplification factors converge 1 as the surface structure fundamental period increases. Besides, the drift and acceleration amplification factors converge 1 as the soil stiffness increases.

The conclusions drawn from the numerical analyses clearly reveal the importance of the dynamic interaction effects between the surface structure and the buried structure. As stated before, the studies in this field are highly case dependent. Therefore, it is apparent that more research is required to present the dynamic interaction effects in other possible cases.

Acknowledgments

The authors would like to thank the reviewers for their valuable and constructive comments which improved the quality of the paper.

References

Abuhajar, O., El Naggar, H. and Newson, T. (2002), "Effects of underground structures on amplification of seismic motion for sand with varying density", 2011 Pan-Am CGS Geotechnical Conference, Ontario, Canada, October.

Abuhajar, O., El Naggar, H. and Newson, T. (2015), "Experimental and numerical investigations of the effect of buried box culverts on earthquake excitation", *Soil Dyn. Earthq. Eng.*, **79**, 130-148, http://dx.doi.org/10.1016/j.soildyn.2015.07.015.

Ahmad, N., Ali, Q., Ashraf, M., Alam, B. and Naeem, A. (2012), "Seismic vulnerability of the Himalayan half-dressed rubble stone masonry structures, experimental and analytical studies", *Nat. Hazards Earth Syst. Sci*., **12**(11), 3441-3454, https://doi.org/10.5194/nhess-12-3441-2012.

Ahmad, N., Shahzad, A., Rizwan, M., Khan, A.N., Ali, S.M., Ashraf, M., Naseer, A., Ali, Q. and Alam, B. (2017), "Seismic performance assessment of non-compliant SMRF reinforced concrete frame: Shake-table test study", *J. Earthq. Eng*., **23**(3), 444-462, https://doi.org/10.1080/13632469.2017.1326426.

Alielahi, H. and Adampira, M. (2016a), "Site-specific response spectra for seismic motions in half-plane with shallow cavities", *Soil Dyn. Earthq. Eng*., **80**, 163-167, http://dx.doi.org/10.1016/j.soildyn.2015.10.003.

Alielahi, H. and Adampira, M. (2016b), "Effect of twin-parallel tunnels on seismic ground response due to vertically in-plane waves", *Int. J. Rock Mech. Mining Sci*., **85**, 67-83, http://dx.doi.org/10.1016/j.ijrmms.2016.03.010.

Alielahi, H., Kamalian, M. and Adampira, M. (2015), "Seismic ground amplification by unlined tunnels subjected to vertically propagating SV and P waves using BEM", *Soil Dyn. Earthq. Eng*., **71**, 63-79, http://dx.doi.org/10.1016/j.soildyn.2015.01.007.

Alielahi, H., Kamalian, M. and Adampira, M. (2016), "A BEM investigation on the influence of underground cavities on the seismic response of canyons", *Acta Geotechnica*, **11**(2), 391-413, https://doi.org/10.1007/s11440-015-0387-7.

Baziar, M.H., Moghadam, M.R., Choo, Y.W. and Kim, D. (2016), "Tunnel flexibility effect on the ground surface acceleration response", *Earthq. Eng. Eng. Vib*., **15**(3), 457-476, https://doi.org/10.1007/s11803-016-0336-y.

Baziar, M.H., Moghadam, M.R., Kim, D.S. and Choo, Y. W. (2014), "Effect of underground tunnel on the ground surface acceleration", *Tunnel. Underground Space Technol*., **44**, 10-22, http://dx.doi.org/10.1016/j.tust.2014.07.004.

Besharat, V., Davoodi, M. and Jafari, M.K. (2012), "Effect of underground structures on free-field ground motion during earthquakes", *The 15th World Conference on Earthquake Engineering*, Lisboa, Portugal, September.

Courant, R., Friedrichs, K. and Lewy, H. (1967), "On the partial difference equations of mathematical physics", IBM J., **3**, 215-234, https://doi.org/10.1147/rd.112.0215.

Doyle, J.F. (1989), "Wave Propagation in Structures: An FFT-Based Spectral Analysis Methodology", Springer, New York, NY, U.S.A.

Franza, A., Marshall, A., M. Haji, T., Abdelatif, A.O., Carbonari, S. and Morici, M. (2017), "A simplified elastic analysis of tunnel-piled structure interaction", *Tunnel. Underground Space Technol*., **61**, 104-121, http://dx.doi.org/10.1016/j.tust.2016.09.008.

Liang, J., Zhang, J. and Ba, Z. (2012), "The effect of underground cavities on design seismic ground motion", *The 15th World Conference on Earthquake Engineering*, Lisboa, Portugal, September.

Jafarnia, M. and Varzaghani, M.I. (2016), "Effect of near field earthquake on the monuments adjacent to underground tunnels using hybrid FEA-ANN technique", *Earthq. Struct*., **10**(4), 757-768, http://dx.doi.org/10.12989/eas.2016.10.4.757.

Joyner, W.B. and Chen, A.T.F. (1975), "Calculation of nonlinear ground response in earthquakes", *Bull. Seismol. Soc. Ame*., **65**(5), 1315-1336.

Lee, C.J., Jeon, Y.J., Kim, S.H. and Park, I.J. (2016), "The influence of tunnelling on the behaviour of pre-existing piled foundations in weathered soil", *Geomech. Eng*, **11**(4), 553-570, http://dx.doi.org/10.12989/gae.2016.11.4.553.

Lysmer, J. and Kuhlemeyer, R.L. (1969), "Finite dynamic model for infinite media", *J. Eng. Mech. Div*., **95**, 859-878.

McKenna, F., Scott, M.H. and Fenves, G.L. (2010), "Nonlinear Finite-Element analysis software architecture using object composition", *J. Comput. Civil Eng*., **24**(1), 95-107, https://doi.org/10.1061/(ASCE)CP.1943-5487.0000002.

Pitilakis, K., Tsinidis, G., Leanza, A. and Maugeri, M. (2014), "Seismic behaviour of circular tunnels accounting for above ground structures interaction effects", *Soil Dyn. Earthq. Eng*., **67**, 1-15, http://dx.doi.org/10.1016/j.soildyn.2014.08.009.

Rizwan, M., Ahmad, N. and Khan, A.N. (2019), "Seismic performance of RC frame having low strength concrete: Experimental and numerical studies", *Earthq. Struct*., **17**(1), 75-89, https://doi.org/10.12989/eas.2019.17.1.075.

Rostami, A., Ziarati, M.A., Shahi, B. and Jahani, S. (2016), "Evaluation of seismic behavior and Earth's surface acceleration, by interaction of tunnels with different shapes and different types of soils", *Open J. Civil Eng*., **6**, 242-253, http://dx.doi.org/10.4236/ojce.2016.62022.

Safak, E. (1999), "Wave-propagation formulation of seismic response of multistory buildings", *J. Struct. Eng*., **125**(4), 426-437, https://doi.org/10.1061/(ASCE)0733-9445(1999)125:4(426).

Sgarlato, G., Lombardo, G. and Rigano, R. (2011), "Evaluation of seismic site response nearby underground cavities using earthquake and ambient noise recordings: A case study in Catania area, Italy", Eng. Geology, **122**(3-4), 281-291, https://doi.org/10.1016/j.enggeo.2011.06.002.

Sica, S., Russo, A.D., Rotili, F. and Simonelli, A.L. (2014), "Ground motion amplification due to shallow cavities in nonlinear soils", **71**, 1913-1935, https://doi.org/10.1007/s11069-013-0989-z.

Sisman, R. and Ayvaz, Y. (2019a), "Comparative modelling of soil – underground structure – surface structure interactions", International Civil Engineering and Architecture Conference, Trabzon, Turkey, April.

Sisman, R. and Ayvaz, Y. (2019b), "Effect of mass ratio on racking ratios of underground structures under seismic loading", International Civil Engineering and Architecture Conference, Trabzon, Turkey, April.

Smerzini, C., Avilés, J., Paolucci, R. and Sánchez-Sesma, F. J. (2009), "Effect of underground cavities on surface earthquake ground motion under SH wave propagation", *Earthq. Eng. Struct. Dyn*., **38**(12), 1441-1460, https://doi.org/10.1002/eqe.912.

Smerzini, C., Avilés, J., Sánchez-Sesma, F.J. Paolucci, R., Santini, A. and Moraci, N. (2008), "Analytical solutions for the seismic response of underground structures under SH wave propagation", AIP Conference Proceedings, Reggio Calabria, Italy, July.

Tsinidis, G. (2017), "Response characteristics of rectangular tunnels in soft soil subjected to transversal ground shaking", *Tunnel.Underground Space Technol*., **62**, 1-22, http://dx.doi.org/10.1016/j.tust.2016.11.003.

Tsinidis, G. (2018), "Response of urban single and twin circular tunnels subjected to transversal ground seismic shaking", *Tunnel. Underground Space Technol*., **76**, 177-193, https://doi.org/10.1016/j.tust.2018.03.016.

Tsinidis, G. and Pitilakis, K. (2018), "Improved R-F relations for the transversal seismic analysis of rectangular tunnels", *Soil Dyn. Earthq. Eng*., **107**, 48-65, https://doi.org/10.1016/j.soildyn.2018.01.004.

PEER Ground Motion Database - PEER Center (2019), PEER Ground Motion Database, UC Berkeley, Californina, USA. https://ngawest2.berkeley.edu/.

OpenSeesWiki (2019), "OpenSeesWiki", UC Berkeley, Californina, USA. http://opensees.berkeley.edu/wiki/index.php/PressureIndependMultiYield_Material.

TBEC (2018), "Turkish building earthquake code", Disaster and Emergency Management Presidency; Ankara, Turkey.

Uang, C.M. and Maarouf, A. (1994), "Deflection amplification factor for seismic design provisions", *J. Struct. Eng*., **120**(8), 2423-2436, https://doi.org/10.1061/(ASCE)07339445(1994)120:8(2423).

Wang, G., Yuan, M., Miao, Y., Wu, J. and Wang, Y. (2018), "Experimental study on seismic response of underground tunnel-soil-surface structure interaction system", *Tunnel. Underground Space Technol*., **76**, 145-159, https://doi.org/10.1016/j.tust.2018.03.015.

Wang, H., Lou, M., Chen, X. and Zhai, Y. (2013), "Structure-soil-structure interaction between underground structure and ground structure", *Soil Dyn. Earthq. Eng*., **54**, 31-38, http://dx.doi.org/10.1016/j.soildyn.2013.07.015.

Wang, H., Lou, M. and Zhang, R. (2017), "Influence of presence of adjacent surface structure on seismic response of underground structure", Soil Dyn. Earthq. Eng., **100**, 131-143, http://dx.doi.org/10.1016/j.soildyn.2017.05.031.

Xu, Z., Du, X., Xu, C., Hao, H., Bi, K. and Jiang, J. (2019), "Numerical research on seismic response characteristics of shallow buried rectangular underground structure", *Soil Dyn. Earthq. Eng*., **116**, 242-252, https://doi.org/10.1016/j.soildyn.2018.10.030.

Yiouta-Mitra, P., Kouretzis, G., Bouckovalas, G. and Sofianos, A. (2007), "Effect of underground structures in earthquake resistant design of surface structures", Geo-Denver 2007: New Peaks in Geotechnics, 1-10, Denver, Colorado, USA, February.

Zidan, A.F. and Ramadan, O.M. (2018), "A hybrid MC-HS model for 3D analysis of tunnelling under piled structures", *Geomech. Eng*., **14**(5), 479-489. https://doi.org/10.12989/gae.2018.14.5.479.

KT